# Methodology for Bare Soil Detection and Discrimination by Landsat TM Image

José A.M. Demattê[*,1], Alfredo R. Huete[2], Laerte Guimarães Ferreira Jr.[2], Marcos Rafael Nanni[3], Marcelo Cardoso Alves[4] and Peterson Ricardo Fiorio[5]

[1]*Department of Soil Science, University of São Paulo, Av. Pádua Dias, 11, Piracicaba, Brazil*

[2]*Department of Soil, Water and Environmental Science, University of Arizona, Tucson, Arizona, USA*

[3]*Department of Agronomy, University of Maringá, Av. Colombo, 5790, Maringá, Brazil*

[4]*Department of Agriculture Information Systems, University of São Paulo, Av. Pádua Dias, 10, Piracicaba, Brazil*

[5]*Department of Agricultural Engeneering, University of São Paulo, Av. Pádua Dias, 10, Piracicaba, Brazil*

**Abstract:** The objective of this work was to develop and test a remote sensing technique to determine bare soils with pixel information from satellite images. The methodology was tested and improved on a 2,805 km$^2$ area located in the state of São Paulo, Brazil. The pixel data from a Landsat-5/TM image was transformed into reflectances. 294 pixels were evaluated by five factors simultaneously and included the following: color composition image; vegetation index; soil brightness information (soil line concept), and a comparison between spectral curve of the pixel with spectral patterns of soils. A validation procedure was based on the discriminate analysis for the real soil related with each pixel. For this, a soil map was overlaid onto the image, and the pixels were related to its respective soil class. Soil brightness variations were readily observed in the spectral curves and in red-NIR features and corresponded to differences in texture and particle size as well in iron and organic matter content. Although qualitative, the observation of color composition was useful for pixel identification. The soil line concept was very useful as it presented a high $R^2$ coefficient (0.90). Comparison between ground level soil spectral curves with satellite information could assist on the evaluation of the real format of the curves. Discriminate analysis indicated a 99.3% correct classification of the soils. Field work validation indicated 90% significance. The present method could help researchers acquire valuable information (i.e., soil attributes quantification), when soil data must be acquired from satellite images.

**Keywords**: Soils, Remote sensing, Reflectance, Discrimination.

## INTRODUCTION

Traditional laboratory soil analyses are expensive, time-consuming, and require unfriendly chemical products with environment alteration. Therefore, the use of alternative "environmentally clean" techniques, such as remote sensing, has become increasingly popular in the agronomy community for soil evaluation and textural classification [1], soil discrimination [2] and intensive agriculture practices (e.g., precision agriculture).

The remotely acquired data and their relationships with soil mineralogy, texture organization, and pedogenetic process have been well demonstrated by numerous studies. Nevertheless, the majority of these studies are based on the use of ground spectral data obtained either under lab conditions or directly in the field [3-5]. Recently, others have tried to apply laboratory spectral analysis methodologies for use in soil surveying [6].

Unlike ground or airborne spectroradiometric data, current satellite data present a much lower spectral resolution. In addition, there are undesirable factors affecting resolution such as landscape and vegetation cover, as well as the intimate mixing of soils and other components within a single pixel. Therefore, before satellite images can be utilized for soil evaluations, we need to know if the pixel data is really from the soil.

The importance of utilizing remote sensing to improve the use of soil is described by [7]. Then, how can we recognize a soil if the spectral data is mixed with plant information? Most studies have used vegetation indexes to identify bare soil [8]. However, these indexes were developed to indicate vegetation and not bare soils. Other field components can interfere with these determinations such as roughness, moisture and landscape position. Therefore, the question remains: "when we study an image obtained from a distance of 800 km from the target (i.e., by satellite), can we extract data that truly pertain to the soil?" If not, all our data regarding this subject must be questioned.

In a pioneer study, [9] tried to quantify soil attributes by satellite images, but obtained only a low correlation between soil attributes and spectral reflectance. They hypothesized that "The low coefficients observed could be attributed to atmospheric particles that are known to affect the electro-

*Address correspondence to this author at the Department of Soil Science, University of São Paulo, Av. Pádua Dias, 11, Piracicaba, Brazil;
E-mail: jamdemat@esalq.usp.br

1875-4139/09 

magnetic energy that is sensed from satellite and aircraft platforms." Furthermore, other factors such as surface conditions with in atmospheric corrections can also interfere in the data collection from image pixels.

One of the first methods to determine bare soil was to look at the real color composition. Although, this method was not quantitative, when used separately it could induce errors. Afterwards, the vegetation index was developed and later followed by the soil line concept [10]. Although, these techniques were used separately for soil identification. An accurate and complete system for the evaluation of satellite images would greatly assist researchers.

Therefore, the main objective of this work was to develop and test a methodology to detect bare soil in satellite images. The main hypothesis was that an accurate remote sensing capacity for the evaluation of various aspects related to soils and satellite image could be correlated with real information. This methodology could be helpful for the scientific community in various ways by allowing the remote detection of soil attributes, such as mineralogy, texture, chemistry, color, quantification and discrimination, to be used to assist soil surveying.

## MATERIALS AND METHODS

For this study, a high productive agriculture region was chosen in the western region of the state of São Paulo, Brazil (Fig. **1**). There were two phases in this study: (1) Development of a method to collect the best pixel data that represent soil information acquired from satellite images; and (2) validation of the method by looking to see if the soils could

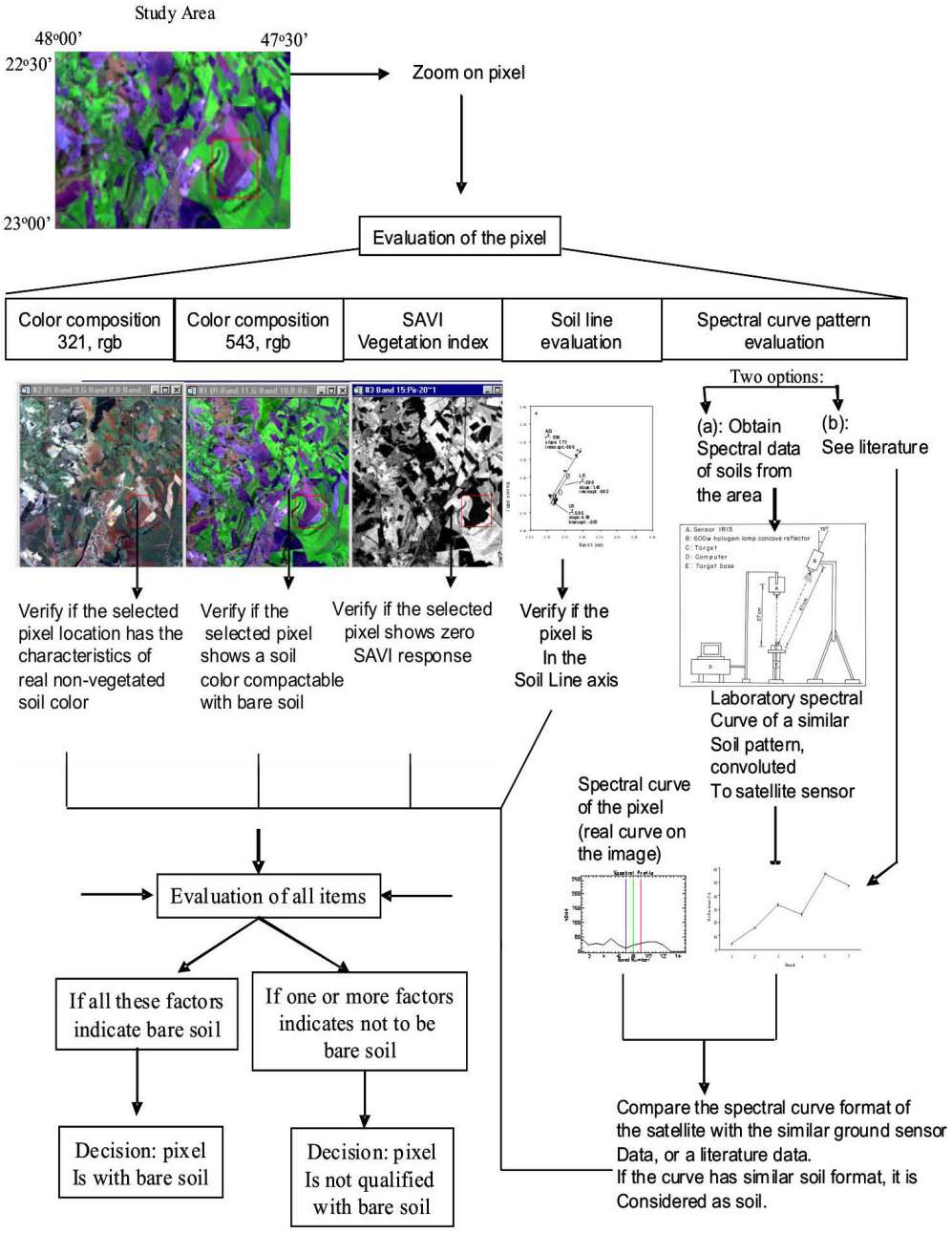


**Fig. (1).** Flow chart of the method to detect bare soil in satellite image.

really be discriminated in unknown locations of the study region.

**Phase One – The Method, Acquisition of Soil Information at the Satellite Level**

A Landsat 5 – TM satellite image with the software ENVI was used. The TM digital numbers were first normalized to the "top of atmosphere" apparent reflectance that was then converted to corrected reflectance with the 6S radiative transfer code simulation [11, 12] to eliminate the effects of Raleigh scattering and ozone absorption:

$$L_{s(\lambda)} = n_1 + m_1 \times DN_\lambda \quad \rho_{app} = \frac{L_{s\lambda} \times \pi}{E_{0,\lambda}} \Rightarrow \frac{L_{s\lambda} \times \pi \times d^2}{E_{0,\lambda} \times \cos(\theta_z)}$$

$$\rho^* = \frac{\frac{\rho_{app}}{t_{o3}} - \rho_{a,r}}{T_r}, \text{ where:}$$

$\mathbf{L_{s\,(\lambda)}}$ ($W/m^2/\mu m$) is the radiance at the sensor; $\mathbf{DN_{(\lambda)}}$ is the digital number for one TM band; **n**, **m** are the TM offset and gain calibration coefficients, respectively; $\boldsymbol{\rho_{app}}$ is the "top of atmosphere" apparent reflectance; $\mathbf{E_{0\lambda}}$, is the solar exo-atmospheric irradiance related to each TM spectral interval; $\boldsymbol{\theta z}$ is the solar zenith angle; **d** is the Earth to sun distance (astronomical units); $\boldsymbol{\rho^*}$ is the Raleigh/Ozone corrected reflectance; $\mathbf{T_{o3}}$ is the ozone transmittance (absorption); $\boldsymbol{\rho_{a,r}}$ is the Raleigh atmospheric reflectance, and $\mathbf{T_r}$ is the total atmospheric Raleigh transmittance. The TM calibration coefficients utilized in this paper were those provided by Dr. Kurt Thome (Remote Sensing Group – Optical Science/University of Arizona, USA).

Reflectance data for the pixels were then collected from images of the studied region. The main point of the methodology is the care that must be used to make the correct evaluation of the pixel. The choice of the pixels used for the verification samplings was based on a series of steps to detect bare soil (see also Fig. **1**):

1. First, the pixel was visually evaluated for color composition information. Two color compositions of the Landsat bands, 3, 2, 1 and 5, 4, 3, red, green, and blue, respectively, were evaluated. The evaluation of the pixel in the first color composition was to look for the real color of the soil. If the pixel information indicated bare soil, it was considered to be so. The second color composition when indicating bare soil presented various tones of purple. Both criteria had to be met for the information to indicate bare soil.

2. The same pixel was evaluated by a vegetation index "Soil Adjust Vegetation Index" (SAVI) [8]. When the value of the index SAVI for the pixel was zero, it was considered as an indicator of bare soil, without vegetation. Therefore,

$$SAVI = \left[ \frac{IVP - V}{(IVP + V + 0.5)} \right] * 1.5$$

where: ***IPV*** is the reflectance in the infrared band (band 4 of Landsat 5 TM) and ***V*** is the reflectance in the red band (band 3). The 0.5 and 1.5 values are the gain and off-set coefficients.

3. For the third step, a dispersion graph (scatter plot) of reflectance values between bands 4 (Near Infra Red) and 3 (Red) representing the "soil line" was made [10, 13]. This graph presented several points that existed in the image, and that reflected the relationship between these two bands. Basically, the brightness was detected. The "soil line" (or 1:1 line) is a line starting between the "x" and "y" axis at a 45-degree angle. As values get closer to the 1:1 line, the probability that the pixel represents bare soil also becomes higher. All points located near this line were marked and the software indicated the respective pixels in the image. Pixels with a higher probability of representing bare soil could then be visualized in the satellite image.

4. A spectral curve for each pixel was directly determined by the software ENVI [14]. This allows the user to retrieve the general spectral patterns of soils. By comparison, the spectral curve could be used to indicate some soil type or be used for another objective. At this point, the user has two options: (a) evaluate spectral curves of soils in the literature or (b) obtain spectral curves of the soils in the region through laboratory analysis. In the case of the present work, we used option "b", and the method used was developed as follows.

**Laboratory Spectral Data of Soils**

In this phase, 39 locations that represent positions of the different soil classes that occur in the study area were evaluated. The objective of this phase was to give to the user an indication of the soil spectral patterns that occur in the region. For the end user, this phase is necessary only if there are no soil spectral data patterns for the region. Usually, this information is accessible from other research studies or from databank patterns. Soil samples were collected from each point of the 39 locations of the different soil classes. Each point was georeferenced using the differential global positioning system (DGPS) with a maximum error of 3 meters. At each point, the soil was sampled at 0-20 and 80-100 cm depths, which corresponded to the surface (Epipedon) and sub-surface horizons, if present [2], respectively, with a total of 542 samples. Theses samples were used for soil classes' designation and bi-directional reflectance measurements in as for Epipedon only.

The collected soil samples were sent for physical, chemical, and mineralogical analysis in the laboratory. Soil samples were taken to laboratory where they were dried at 45°C for 48 h and sieved to 2 mm. The texture groups of the soils were defined according to [15]. The contents of total sand, silt, and clay were determined by the densimeter method [16]. The texture ratio was defined by dividing the mean values of the clay contents found in the A and A/B horizons (when present) by the contents of clay from the B horizon, with the exception of the BC horizon [15]. Soil chemical analyses included pH (using $CaCl_2$ solution 0.01 N), organic matter, OM (Colorimeter method), phosphorus, calcium, magnesium and potassium (extracted by the ion-exchange resin method), and aluminum (using extractor KCl, 1 N) and aluminum plus hydrogen (using SMP buffer solution with calcium acetate, 1 N, pH 7.0) were determined [17]. Total iron was determined

by the sulfuric acid digestion method [16]. Munsell colors were used to characterize the dry and moist soil samples by colorimeter method. Mineralogical analyses of the sand, silt, and clay fractions were performed [18].

Soil samples were oven-dried, crushed, and sieved (2 mm). Bi-directional reflectance measurements (450-2500 nm) of the fine earth material were carried out using a laboratory spectroradiometer, Infra-red Intelligent Spectroradiometer, with the sensor positioned vertically at a distance of 27 cm over the soil sample. The samples were placed on a 9-cm diameter Petri dish. The light source, a 650-W halogen lamp, was positioned 61 cm from the sample container at a $15^{o}$-zenith angle. The energy for the lamp was controlled by regulated voltage equipment. A white calibrated plate ($BaSO_4$) was used as the primary standard. Spectral curves were correlated with the classification obtained in the field, thus giving the spectral soil pattern. This information was converted into satellite sensor data to facilitate its interpretation. A simulation was established to compare satellite and terrestrial data. The mean SR factor obtained by the IRIS sensor was calculated in the wavelength ranges corresponding to sensor bands (convolution), e.g., 450–520, 520–600, 630–690, 760–900, 1,550–1,750, and 2,080–2,350 nm. A Tukey test between each band was performed to evaluate which bands could differentiate the soils. Soils discriminate analyses [2], were also developed with the DISCRIM procedure [19]. The objective of these results was to verify if their reflectance would influence their discrimination. This information could be useful to understand the satellite data.

Therefore, an image pixel was considered to be bare soil only if all four items discussed indicated so. The complete method is illustrated in Fig. (**1**).

## Phase Two: Validation Procedure

There were used two procedures do validate the methodology. The first method had as objective to collect spectral pixel information (using the methods of phase 1). The pixel information would then be inserted into discriminate analyses for the soil spectral data. It was considered that if this information was from bare soil, then the soils could be discriminated. Thus, an atmosphere-corrected scene was overlaid with vector file (semi-detailed soil map) where we had sampled 26 soils types in all regions. Afterwards, was followed phase one steps, and evaluated 294 soil spectral samples (pixels) that had their spectral data extracted. The position of the pixel was evaluated in relationship to the limits of the soil type in a semi-detailed survey looking for the pixels located inside the mapping units studied.

The major soil types encountered in the study region and utilized in this investigation are indicated in Table **1**. In each of these types, there were subgroups that (according to Brazilian Classification System) were also evaluated, for example, LV1, LV2, LV3, which are discussed in the text, difference in their parental material, granulometric and/or chemical characteristics. The 294 soil data pixels were then grouped into the soil types based on the soil map. Therefore, several pixels belonged to each of the respective soil classifications. These data were then subjected to non-parametric discriminate analysis [19]. The validation procedure expected that if soils were well discriminated, then their pixel data were from bare soils (Fig. **2**).

To ensure a stronger validation for the method field work was developed. 100 field locations (100 hundred from the 294 hundred) where pixels were collected, were visited with a GPS at the field to check surface situation. It was consid-

**Table 1. Soil Classification and Designation**

| Soil Classification | | Abbreviation | Observation Landscape | Drainage | Depth (cm) | Color[c] |
|---|---|---|---|---|---|---|
| American[a] | Brazilian[b] | | | | | |
| Typic Eutrorthoxs, Pachic Umbriorthoxs | Latossolo Vermelho distroférrico | LR | Flat to gently rolling | Well | > 200 | 1.3 YR 3.3/2.3 |
| Rhodic Paleudalfs | Nitossolo Vermelho | TR | Gently rolling to rolling | Moderate | > 200 | 2.5 YR 3.1/2.8 |
| Typic Haplorthoxs | Latossolo Vermelho | LE | Flat to gently rolling | Well to strong | > 200 | 2.5YR 3/3 |
| Typic Haplorthoxs, Typic Umbriorthoxs, Pachic Umbriorthoxs | Latossolo Vermelho Amarelo | LV | Flat to gently rolling | Well to strong | > 200 | 4.9 YR 3.5/2.9 |
| Typic Paleudults, Typic Paleudalfs | Argissolo Vermelho | PE | Rolling | Moderate | > 200 | 2.5 YR 3.3/2.9 |
| Paleudults, Arenic Abruptic Paleudalfs, Typic Paleudalfs, Abruptic Paleudalfs and Abruptic Arenic Paleudults (PV) | Argissolo Vermelho Amarelo | PV | Rolling | Moderate | > 200 | 3.9 YR 3.3/2.5 |
| Typic Udorthents and Lithic Hapludolls | Neossolo Litólico | Li | Strong rolling | Ob-structed | < 30 | 2.5 YR 3.3/2.8 |
| Typic Quartzipsamments | Neossolos Quart-zarênico | AQ | Flat to gently rolling | Very Strong | >200 | 7.7 YR 3.7/2.6 |
| Albiaquic Paleudalfs, Vertic Paleudalfs and Epiaquic Tropuldults | Planossolo | PL | Flat to gently rolling | Worth | >200 | |
| Aquoxs, Aquults, Aquepts and Aqualf | Gleissolo | G | Flat | Very Worth | >200 | 8.9YR 4.5/2.9 |

[a] Soil Survey Staff (1998).
[b] Brazilian Soil Classification (Embrapa, 1999).
[c] Minolta Colorimeter based on the Munsell Color Charts, Baltimore, Maryland, U.S.A., 1954.

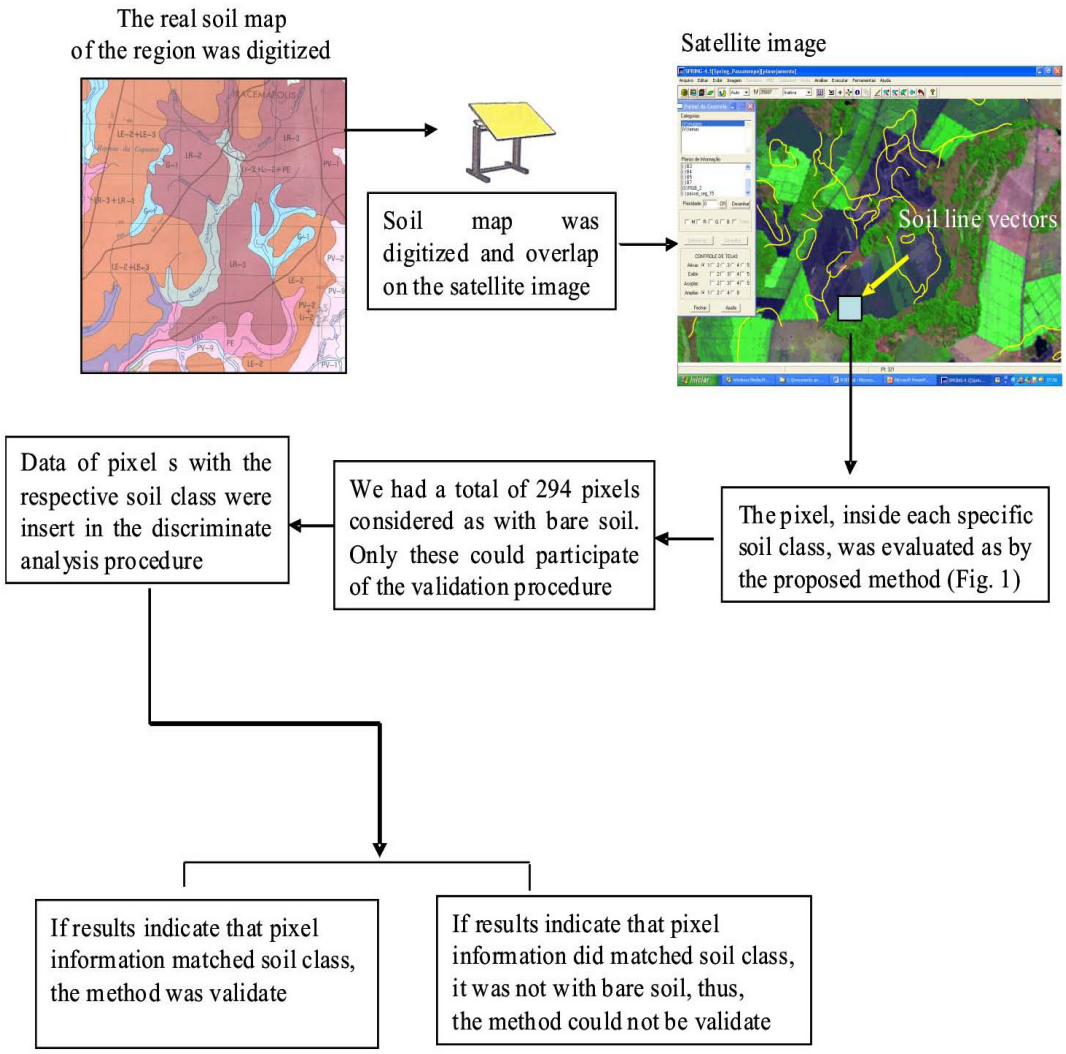


**Fig. (2).** Sequence of the validation procedure.

ered three types of situation, vegetated, partially vegetated, non vegetated (bare soil). A statistics of error was performed. We considered only non-vegetated as correct samples.

## RESULTS AND DISCUSSION

### Pattern of Soils Obtained by Laboratory Spectroradiometric Data

Before exploring remote sensing techniques, it is important to understand the spectral behavior of soils at the ground level. Spectral signature curves for the different soil types are shown in Fig. (**3a**). Conspicuous differences in the reflectance intensities or brightness, particularly in the spectral interval between 850 to 2350 nm, could be observed. Besides the typical absorption features, there were vibration modes (e.g., Al-OH bending mode near 2,100 nm and $OH^-$ overtones near 1,400 and 1,900 nm) and electronic transitions (e.g., $Fe3^+$ crystal field electronic features near 410 nm). These variations in brightness clearly corresponded to a decrease in the clay content as well as in the total iron content as the soil sequence (LR, TR, PE, LE, PV, AQ) becomes more sandy, with quartz dominating (mineralogical analysis) and becoming brighter (Table **2**). Quartz improves the reflectance intensity of soils [20]. Also, weathered soils such as LR presented absorption band at 2,265 nm, which indicates the presence of gibbsite that can be confirmed by X-ray analysis, and shows an absorption feature that can discriminate this soil from others [21].

The LR and TR soils, which have the highest clay and iron contents, show the lowest brightness and nearly flat spectral signature curves (Table **2**). The absorption features, specially the vibration tones, are masked by opaque and trans-opaque minerals, mainly magnetite and ilmenite as suggested by the X-ray diffraction analysis [22]. Statistically speaking, these two soils show similar spectral behavior, which prevents practical discrimination when considering the TM spectral intervals (Table **3**). Similar spectral behavior, concerning the TM intervals and statistical significance, was also observed between the PE and LE soils, even though the LE soil tends to show a more abrupt reflectance increase beyond 1,000 nm. Spectral similarity was also found between the TR and PE soils [5]. This is somewhat expected since these two soils are derived from basaltic parent material and have high opaque minerals contents in the sand fraction, which results in low brightness and causes the absorp-

tion features to be rather indistinguishable [22]. Nevertheless, it is important to note that slight differences in the reflectance values are at around the TM-5 interval. Higher values found in the PE soil are attributed to alterations in the iron content and texture as well. These two soils are very similar in the field, and sometimes only the iron contents can discriminate them ($Fe_2O_3$ > 120 g $kg^{-1}$ for TR).

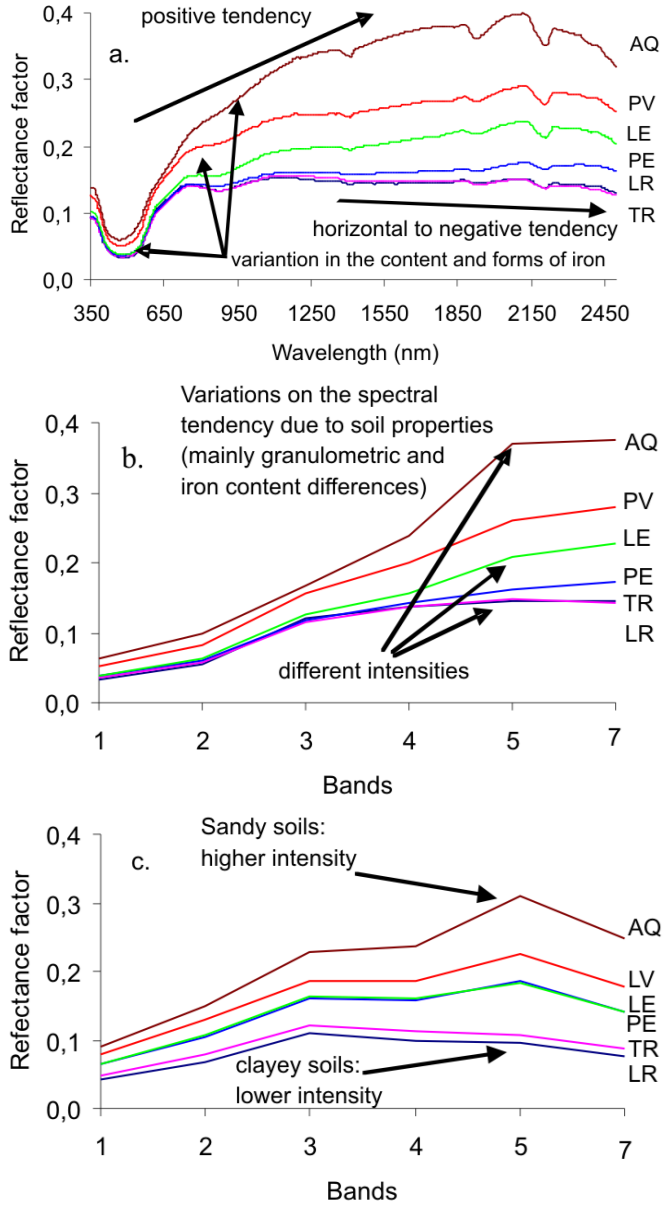


**Fig. (3).** Ground (laboratory) spectral curves of soil (**a**); Simulated spectral data; (**b**) Real TM spectral data for soils (**c**).

The occurrence of crystalline iron, mainly as ferric oxides, is primarily confirmed by the well-defined absorption features observed in the 400-500 nm intervals [23]. In the studied soil sequence, as the iron content increases from AQ to LR (Table **2**), these concavity features, which are caused by $Fe^{3+} \rightarrow O^{2-}$ charge transfers, become sharper and progressively shifts towards the visible portion of the spectrum. These displacement is related to crystal field transitions, which is intensified by higher levels of $Fe^{3+}$ ion content and anti-ferromagnetic couplings of oxides and hydroxides [24].

**Table 2. Chemical and Textural Soil Data from the Studied Region**

| Soil Expression | Organic Matter | Sand | Silt | Clay | $Fe_2O_3$ [a] |
|---|---|---|---|---|---|
| | ---------- g $kg^{-1}$ ---------- | | | | |
| LR | 15 | 263 | 120 | 616 | 213 |
| TR | 21 | 270 | 180 | 550 | 180 |
| LE | 14 | 542 | 100 | 357 | 94 |
| LV | 16 | 618 | 105 | 278 | 38 |
| PE | 31 | 250 | 160 | 590 | 49 |
| PV | 13 | 701 | 121 | 176 | 50 |
| Li | 28 | 526 | 173 | 286 | 77 |
| AQ | 12 | 850 | 70 | 80 | 18 |
| PL | 22 | 290 | 210 | 500 | 50 |
| G | 39 | 390 | 245 | 365 | 125 |

[a]Total iron extracted by sulfuric acid digestion.

Variations in the iron content as well as in its ionic and crystalline state are also indicated by the absorption features in the 800-900 nm regions. As the soil type becomes sandier, there is less iron to affect the reflectance and these features progressively fade. Concomitantly, the vibration absorption features near 1,400, 1,900, and 2,200 nm become deeper and sharper as the masking factors, mainly iron oxides/hydroxides and organic matter, decrease. This is clearly seen in the spectrum of the highly bright, quartz dominated AQ soil [6].

## Soil Patterns Obtained by Satellite Multispectral Data

The average spectral signature curves simulating Landsat-5 TM (Fig. **3b**) data are different from the ground spectroradiometer data since no specific absorption features can be observed (Fig. **3a**). Nevertheless, spectral characterization and discrimination between soils are still possible since these curves show differences in shape and reflectance intensity [25]. On the other hand, the spectral patterns from laboratory-simulated data were very similar to the real satellite sensor information (Fig. **3c**). The next step should then be to understand and evaluate real satellite information.

As we observed, LR and TR had similar spectral curves. These are clayey to very clayey soils with a high content of hematite, which is responsible for the low reflectance [26]. As the iron content decreases and the sandy texture becomes more pronounced (refer to Table **2**), an increase in brightness is readily observed (PE and LE soils). A further decrease in the iron content concomitant to an increase in the content of sand yields even higher reflectance, especially near the TM 5 spectral interval (LV soil).

Although LR, LE, and LV soils present nearly identical morphological properties (the presence of a B horizon), they do show distinct spectral behaviors. This distinct spectral behavior is mainly attributed to a decrease in the iron content in the sequence LR, LE, LV, which is accompanied by a reflectance increase. In this sequence, soil color ranges from 2.5YR (LR) to 5YR (LV), which is also related to hematite

**Table 3. Statistical Analysis[a] for Spectral Bands from the Laboratory Sensor**

| Soil | Band[b], nm | | | | | | | | | | | |
|---|---|---|---|---|---|---|---|---|---|---|---|---|
| | 1 | | 2 | | 3 | | 4 | | 5 | | 7 | |
| | 450-520 | | 520-600 | | 630-690 | | 760-900 | | 1550-1750 | | 2080-2350 | |
| LR | 0.033 | A* | 0.056 | A | 0.1193 | A | 0.1369 | A | 0.1446 | A | 0.1446 | A |
| TR | 0.035 | A | 0.056 | A | 0.1148 | A | 0.1362 | A | 0.1476 | A | 0.1424 | A |
| PE | 0.0372 | A | 0.0598 | A | 0.1178 | A | 0.1413 | A | 0.161 | A | 0.1715 | AB |
| LE | 0.043 | B | 0.644 | B | 0.1275 | B | 0.1617 | B | 0.2168 | B | 0.23 | B |
| PV | 0.0524 | C | 0.0834 | C | 0.155 | CD | 0.2009 | C | 0.2629 | C | 0.2789 | CD |
| AQ | 0.0624 | C | 0.098 | C | 0.1659 | D | 0.2396 | C | 0.3714 | D | 0.3755 | E |

[a] Tukey test was applied to the reflectance values for each band. Mean values were compared to the spectral data from all soils in each band. Different letters denote a statistically significant difference ($P < 0.01$) between the spectral data of soils in each respective band.
[b] Bands reflect the Landsat-5 TM range. Spectral data simulated from ground base data set.
* Same letter in the column indicates no statistical difference at 5% significance (Tukey test).

and goethite contents, respectively [27]. This variation in hue, which is a direct response to changes in the iron and organic matter contents, is clearly depicted by the TM visible bands [28]. With respect to the soils dominated by a sandy texture in the top layers (LV, PV, Li, and AQ), these soils tend to show a higher overall reflectance, which peaks out in the TM-5 region.

Soil spectra at the series level seem to follow the same trends observed at the lower taxonomic category. As seen in Fig. (**4**), which depicts the spectral signatures of distinct soil types belonging to the LE and LV subgroups, soil brightness variations confirm changes in texture and iron content as previously described. For example, LV5 and LV7 are quite different in the reflectance intensity when compared with LV1 and LV3. This occurs because the first group has higher contents of clay and iron. Also, note that, as sand content increases for the soil unit, reflectance becomes higher in band 5.

With regards to soil discrimination at the subgroup level, no single TM band was capable of simultaneously discriminate all soil types (Table **4**). Nevertheless, partial discrimination with statistical significance was achieved using individual bands. For example, TM-1 throughly separates soils LR, LE, and PV while no clear distinction was made between the LV and LE. It is also worth mentioning that the complete discrimination between LR, LE, and LV throughout the spectral range was evaluated. Therefore, these results can help determine the key bands for the discrimination of tropical soils [29-31].

In spite of the similarities, a major difference between the original and simulated TM curves for the relative reflectance intensity between TM-5 and TM-7 spectral intervals was observed. In the case of the simulated data, from TM-5 to TM-7, the reflectance intensity either shows a slight increase or stays constant, while the original TM data show a negative slope from TM-5 to TM-7. A plausible explanation for this opposite behavior may be associated with the surface reflectance retrieval for TM-7. Water vapor, for which no correction was attempted, may slightly lower the atmospheric transmittance in the 2,080 to 2,350 nm region. In addition, the calibration coefficients utilized to convert the digital numbers to "top of atmosphere" apparent reflectance may not have correctly accounting for sensor degradation and the very low irradiance in the TM-7 range. One must also leave open the possibility of moisture content in both, soil and litter. In this case, TM-7, rather than TM-5, would

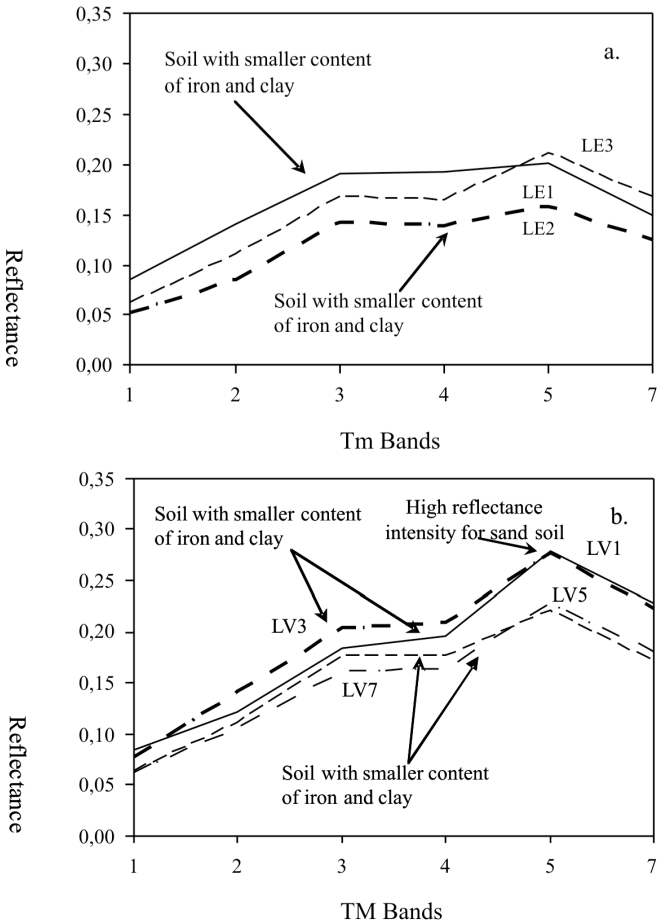


**Fig. (4).** Spectral curves extracted from the TM image of soil series (map units) within the LR (**a**) and LV (**b**) subgroups, respectively.

**Table 4. Statistical Analysis[a] for Spectral Bands of the TM/Landsat-5 (Data Obtained from Orbital Sensor)**

| Soil | Band[b], nm | | | | | | | | | | | |
|---|---|---|---|---|---|---|---|---|---|---|---|---|
| | 1 | | 2 | | 3 | | 4 | | 5 | | 7 | |
| | 450-520 | | 520-600 | | 630-690 | | 960-900 | | 1550-1750 | | 2080-2350 | |
| LR | 0.043 | D* | 0.07 | D | 0.112 | D | 0.100 | D | 0.098 | D | 0.078 | D |
| LE | 0.055 | C | 0.094 | C | 0.151 | C | 0.148 | C | 0.167 | C | 0.124 | C |
| LV | 0.068 | B | 0.115 | B | 0.176 | B | 0.179 | AB | 0.239 | A | 0.189 | A |
| PV | 0.084 | A | 0.135 | A | 0.193 | A | 0.196 | AB | 0.245 | A | 0.195 | A |
| Li | 0.076 | B | 0.123 | B | 0.181 | AB | 0.178 | B | 0.199 | B | 0.158 | B |
| TR | 0.047 | C | 0.077 | C | 0.112 | C | 0.112 | C | 0.106 | C | 0.086 | B |
| PE | 0.064 | CB | 0.104 | CB | 0.159 | BC | 0.157 | BC | 0.185 | B | 0.142 | B |
| AQ | 0.09 | A | 0.116 | AB | 0.173 | BC | 0.253 | A | 0.309 | A | 0.247 | A |
| PL | 0.078 | AB | 0.12 | AB | 0.159 | BC | 0.158 | BC | 0.181 | B | 0.126 | B |
| G | 0.07 | AB | 0.15 | A | 0.229 | A | 0.176 | B | 0.175 | B | 0.134 | B |

[a] Tukey test was applied to the reflectance values for each band. Mean values were compared to the spectral data from all soils in each band. Different letters denote a statistically significant difference ($P < 0.01$) between the spectral data of soils in each respective band.
[b] Bands represent Landsat-5 TM ranges. Spectral data simulated from ground data set.
* Same letter in the column indicates no statistical difference at 5% significance (Tukey test).

preferentially depict the absorption features related to the $OH^-$ groups.

The soil line concept was very useful for the evaluation of the pixel. We first evaluated the ground sensor data. A better insight into the nature and relationships between the distinct soil types was provided by the soil lines plotted in the red-near infrared range (Fig. **5a** and Table **5**). These are best-fitted lines through each red/NIR pair for the large number of soils, which readily yielded information regarding the slope and brightness of each soil spectrum. The statistics are shown in Table **5**. The $R^2$ values were high because they are bare soils, but they do not have the same tendencies (different slope and intercept) (Table **5**) [13, 32].

For soil lines relative to the ground spectroradiometric data and for those based on the TM imagery (Fig. **6**), it was found that ferric oxide dominated soils (LR) are preferentially positioned near the origin of the red-NIR range, while the bright, sand dominated soils (AQ) tend to be further away from the origin. It is also important to emphasize that distinct soil lines were required in order to synthesize the spectral information of each soil type herein considered, being important for the soil discrimination [10, 13, 33]. Differences in line parameters (i.e., slope and intercept) may be regarded as a direct response to the wide variability in the organic matter and iron oxide contents among the major soil types [13].

It is also important to point out that the slopes of the TM data soil lines seem to be systematically lower when compared to the slopes of the "ground data" soil lines. On one hand, the closer proximity of the TM data soil lines to the 1:1 line may strongly suggest that the extracted samples were predominately from bare soil surfaces. However, the points from soils do not match exactly on a 1:1 graphic position and have variability along the soil line, as shown in Fig. (**5**) [32].

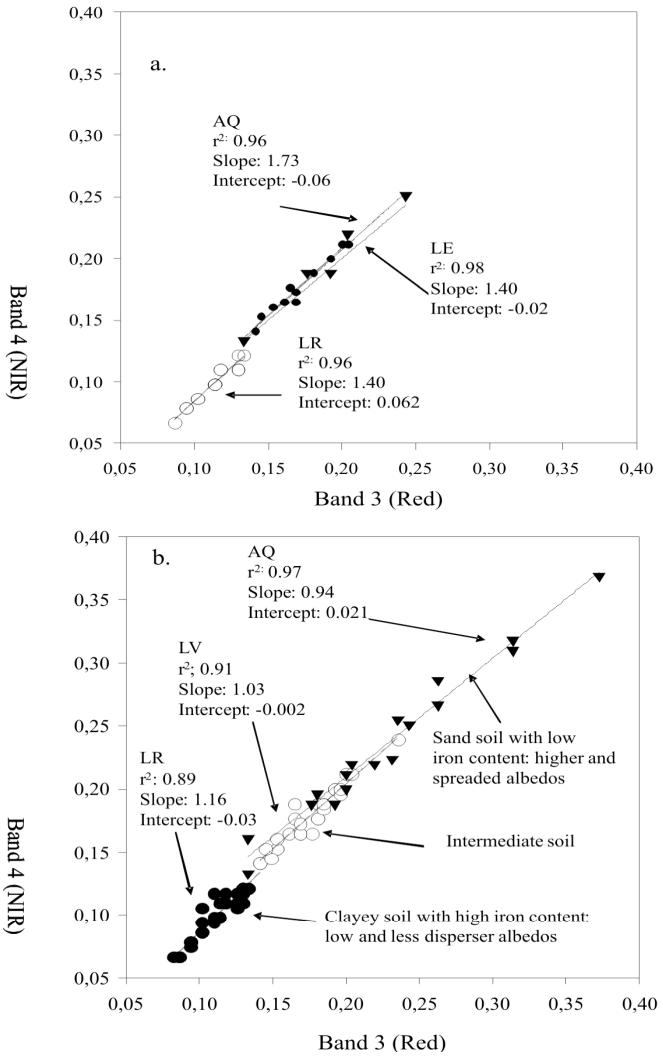


**Fig. (5).** General soil line obtained from: Ground sensor (**a**); Orbital sensor (**b**).

**Table 5. Soil Line Statistical Parameters for Ground and Satellite Sensors**

| Satellite Data - Individual Soil Units | | | | Satellite Data – Overall Group of Soils | | | | Ground Data - Great Groups of Soils | | |
|---|---|---|---|---|---|---|---|---|---|---|
| **Unit** | **Obs.** | **Equation** | **$R^2$** | **Unit** | **Obs.** | **Equation** | **$R^2$** | **Obs.** | **Equation** | **$R^2$** |
| LR1 | 9 | y = 1.236x – 0.039 | 0.99 | LR | 38 | y = 1.163x – 0.03 | 0.89 | 3 | y = 4.09x – 0.352 | 0.91 |
| LR2 | 12 | y = 1.119x –0.024 | 0.84 | | | | | | | |
| LR3 | 17 | y = 0.863x + 0.006 | 0.63 | | | | | | | |
| LE1 | 3 | y = 0.824x + 0.036 | 0.94 | LE | 57 | y = 1.022x –0.006 | 0.94 | 14 | y = 1.40x – 0.020 | 0.98 |
| LE2 | 18 | y = 1.110x – 0.01 | 0.95 | | | | | | | |
| LE3 | 4 | y = 0.977x +0.0009 | 0.99 | | | | | | | |
| LE2+LE3 | 32 | y = 0.945x + 0.005 | 0.91 | | | | | | | |
| LV1 | 5 | y = 0.906x + 0.028 | 0.87 | LV | 28 | y = 1.034x - 0.002 | 0.91 | - | - | - |
| LV3 | 3 | y = 0.969x + 0.011 | 0.99 | | | | | | | |
| LV5 | 12 | y = 0.990x + 0.002 | 0.74 | | | | | | | |
| LV7 | 8 | y = 1.040x + 0.036 | 0.96 | | | | | | | |
| PV1 | 4 | y = 1.157x - 0.036 | 0.71 | PV | 61 | y = 1.054x - 0.008 | 0.96 | 5 | y = 1.453x – 0.018 | 0.99 |
| PV4 | 14 | y = 1.15x - 0.027 | 0.99 | | | | | | | |
| PV6 | 3 | y = 1.164x - 0.098 | 0.99 | | | | | | | |
| PV7 | 27 | y = 0.975x + 0.008 | 0.95 | | | | | | | |
| PV9 | 10 | y = 1.138x - 0.022 | 0.96 | | | | | | | |
| PV11 | 3 | y = 0.601x + 0.078 | 0.95 | | | | | | | |
| Li2 | 3 | y = 0.965x +0.0011 | 0.85 | Li | 30 | y = 1.055x - 0.012 | 0.92 | - | - | - |
| Li3 | 24 | y = 0.971x +0.0001 | 0.95 | | | | | | | |
| Li6 | 3 | y = 0.960x +0.0002 | 0.83 | | | | | | | |
| G1 | 6 | y = 1.589x - 0.077 | 0.55 | G | 11 | y = 1.060x - 0.0042 | 0.95 | - | - | - |
| G3 | 5 | y = 1.082x - 0.011 | 0.99 | | | | | | | |
| - | - | - | - | PE | 20 | y = 0.881x + 0.017 | 0.92 | 5 | y = 0.969x - 0.027 | 0.96 |
| - | - | - | - | PL | 5 | y = 0.25x + 0.1225 | 0.5 | - | - | - |
| - | - | - | - | TR | 20 | y = 1.123x - 0.023 | 0.96 | 6 | y = 1.324x – 0.015 | 0.81 |
| - | - | - | - | AQ | 19 | y = 0.941x + 0.021 | 0.97 | 6 | y = 1.521x – 0.012 | 0.99 |
| | | | | All soils | 289 | y = 1.097x - 0.017 | 0.97 | 39 | y = 1.735x – 0.061 | 0.96 |

Nevertheless, the high $R^2$ values found for all the soil lines reveal that the set of samples within the same subgroup (e.g., LR) depict a broad range in reflectance magnitudes and show good concordance regarding their spectral shapes. Regarding the TM data, minor deviations from the estimated soil lines, as observed in Fig. (**6b**), may be an indication that litter and surface roughness contributions to the pixel response should not be neglected [13].

## Validation of the Method

Concerning the validation analysis, a 100% discrimination was achieved when considering the ground spectroradiometric data (Table **6**). These results were indicative suggesting that similar results could be expected with the satellite data [13]. Similar results [29], although they had errors of 55.6%, which were most likely because they used a field spectral radiometer.

The validation procedure was based on the evaluation of soil discriminate analyses with satellite data. The results indicated that 99.4 % of the samples were correctly classified, considering the 10 major soil types (subgroup level) (Table **7**). The samples that were misidentified occurred between similar soils. For example, LE was confused only once with TR, and one sample of LR with LE [23]. These soils are all similar, and these errors are acceptable. In general LR and TR can only be discriminated by soil profile

morphology evaluation. There were confusions in spectral data classification of soils in transition areas when work with laboratory data [23].

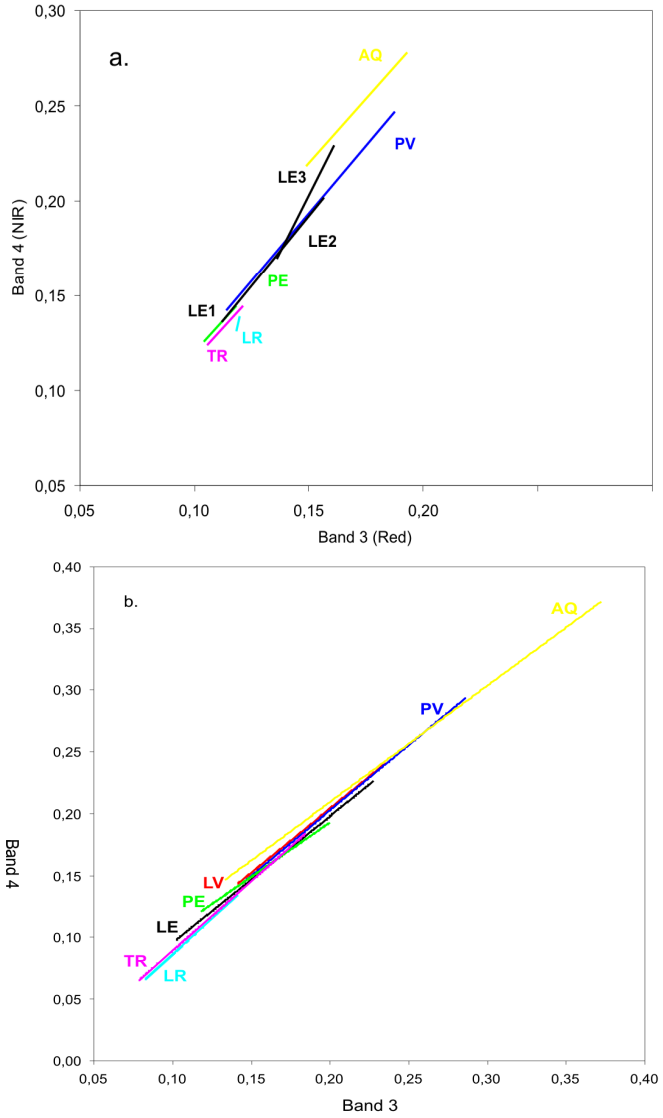


**Fig. (6).** General soil line obtained from ground (**a**) and satellite (**b**) sensors for all studied soils.

The discrimination of 26 map units (series level) showed a high performance with 99.3% correct classification (Table **8**). The few errors observed occurred between similar soils such as LR3 with LR2, which have very similar morphological characteristics.

Field work indicated that the predominant samples visited was non-vegetated soils. From the 100 places visited, 90 had bare soils (places where soil was in preparation for management), and 10 was partially vegetated (with low high of the culture, although with soils in appearance), and none of them had full vegetation. The important here is that the date of the image was from final of September, when we have less influence of humidity and large agriculture areas, where farmers are working on the bare soil. Thus, the date and region of interest are important for the success of the bare soil detection.

## CONCLUSIONS

The coarse resolution of satellite data, although lacking diagnostic absorption features observed in the laboratory soil spectra, readily responded to variations in texture and granulometry, as well as to the iron and organic matter contents. Such responses, generally associated with brightness changes, were clearly depicted in both the spectral curves and the red-NIR ranges.

Real and accurate information from bare soils can be detected by satellite spectral image information by using a simultaneous methodology. The real color compositions allowed factual visual information to be obtained from bare soil. The soil line concept is an important factor for this analysis. Pixels along the soil line demonstrated bare soil and were influenced by soil attributes. The vegetation index also indicated non-bare soil conditions. The use of only one of these parameters does not guarantee bare soil information. The study of the behavior of spectral patterns, before using satellite information, could assist in the collection decision for bare soil pixels.

The methodology was validated with 90% significance on field work and 99.3% of statistical analysis of the collected pixels correctly associated with its respective soil classification. Thus, this method can greatly improve studies where satellite pixel information from bare soil is required.

**Table 6. Non-Parametric Discriminate Analysis for the 6 Units of Soils (Number of Observations and Error for the Classification) for the Ground Spectral Data**

| Soil | Total of Samples | Correct | | Error | | |
|---|---|---|---|---|---|---|
| | | Samples | % | Samples | % | Soil Misidentified |
| AQ | 6 | 6 | 100 | 0 | 0 | - |
| LE | 14 | 14 | 100 | 0 | 0 | - |
| LR | 3 | 3 | 100 | 0 | 0 | - |
| PE | 5 | 5 | 100 | 0 | 0 | - |
| PV | 5 | 5 | 100 | 0 | 0 | - |
| TR | 6 | 6 | 100 | 0 | 0 | - |
| **Total** | **Error** | | **0.0** | | | |

"-" Does not exist.

**Table 7. Non-Parametric Discriminant Analysis for the 10 Main Groups of Soils, Number of Observations, Classifications and Error for Data Obtained from Satellite Sensor**

| Soil | Total of Samples | Correct Samples | % | Samples | Error % | Soil Confused |
|---|---|---|---|---|---|---|
| AQ | 19 | 19 | 100 | 0 | 0 | - |
| G | 11 | 11 | 100 | 0 | 0 | - |
| LE | 57 | 56 | 98 | 1 | 1.75 | TR |
| LR | 38 | 37 | 97.37 | 1 | 2.63 | LE |
| LV | 28 | 28 | 100 | 0 | 0 | - |
| Li | 30 | 30 | 100 | 0 | 0 | - |
| PE | 18 | 18 | 100 | 0 | 0 | - |
| PL | 5 | 5 | 100 | 0 | 0 | - |
| PV | 61 | 60 | 98.36 | 1 | 1.64 | G |
| TR | 20 | 20 | 100 | 0 | 0 | - |
| **Total** | **Error** | | **0.6** | | | |

"-" not exist.

**Table 8. Non-Parametric Discriminate Analysis for the 26 Units of Soils (Number of Observations and Error on the Classification) for Data Obtained from Satellite Sensor**

| Soil | Total of Samples | Correct Samples | % | Samples | Error % | Soil Confused |
|---|---|---|---|---|---|---|
| AQ | 19 | 19 | 100 | 0 | 0 | - |
| G1 | 6 | 6 | 100 | 0 | 0 | - |
| G3 | 5 | 5 | 100 | 0 | 0 | - |
| LE1 | 3 | 3 | 100 | 0 | 0 | - |
| LE2 | 18 | 18 | 100 | 0 | 0 | - |
| LE2+LE3 | 32 | 32 | 100 | 0 | 0 | - |
| LE3 | 4 | 4 | 100 | 0 | 0 | - |
| LR1 | 9 | 9 | 100 | 0 | 0 | - |
| LR2 | 12 | 12 | 100 | 0 | 0 | - |
| LR3 | 16 | 15 | 88.24 | 1 | 5.88 | LR2 |
| LV1 | 5 | 5 | 100 | 0 | 0 | - |
| LV3 | 3 | 3 | 100 | 0 | 0 | - |
| LV5 | 12 | 12 | 100 | 0 | 0 | - |
| LV7 | 8 | 8 | 100 | 0 | 0 | - |
| Li2 | 3 | 3 | 100 | 0 | 0 | - |
| Li3 | 24 | 24 | 100 | 0 | 0 | - |
| Li6 | 3 | 3 | 100 | 0 | 0 | - |
| PE | 18 | 18 | 100 | 0 | 0 | - |
| Pl | 5 | 5 | 100 | 0 | 0 | - |
| PV1 | 4 | 4 | 100 | 0 | 0 | - |
| PV11 | 3 | 3 | 100 | 0 | 0 | - |
| PV4 | 14 | 14 | 100 | 0 | 0 | - |
| PV6 | 3 | 3 | 100 | 0 | 0 | - |
| PV7 | 27 | 26 | 96.3 | 1 | 3.7 | LE1 |
| PV9 | 10 | 10 | 100 | 0 | 0 | - |
| TR | 19 | 18 | 95 | 1 | 5 | LE2 |
| **Total** | **Error** | **0.7** | | | | |

"-" not exist.

## ACKNOWLEDGMENTS

We thank the São Paulo State Science Foundation (FAPESP) for their financial support (95/6259-6; 95/9641-91998/1059-7) and CNPq (300371/96-9) for this work and Dr. Kurt Thome (Remote Sensing Group – Optical Science / University of Arizona, USA) for the calibration data coefficients.

## REFERENCES

[1] Shephered KD, Walsh MG. Development of reflectance spectral libraries for characterization of soil properties. Soil Sci Soc Am J 2002; 66: 988-98.

[2] Nanni MR, Demattê JAM, Fiorio PR. Soil discrimination analysis by spectral response in the ground level. Pesqui Agropecu Bras 2004; 39: 995-1006.

[3] Huete AR, Escadafal R. Assessment of biophysical soil properties through spectral decomposition techniques. Remote Sens Environ 1991; 35: 149-59.

[4] Epema GF, Bom CJB. Spatial and temporal variability of field reflectance as a basis for deriving soil surface characteristics from multiscale remote sensing data in Niger. ITC J 1994; 1: 23-8.

[5] Nanni MR, Demattê JAM. Spectral reflectance methodology in comparison to traditional soil analysis. Soil Sci Soc Am J 2006; 70: 393-407.

[6] Demattê JAM, Campos RC, Alves MC, Fiorio PR, Nanni MR. Visible-NIR reflectance: a new approach on soil evaluation. Geoderma 2004; 121: 95-112.

[7] Andronikov VL, Dobrovol'skiy GV. Theory and methods for use of remote sensing in the study of soils. Mapping Sci Remote Sens 1991; 28: 92-101.

[8] Huete AR. Soil Influences in Remotely Sensed Vegetation-Canopy Spectra. In: Ghassem A, Ed. Theory and Application of Optical Remote Sensing. John Wiley and Sons: New York 1989; pp. 107-41.

[9] Coleman TL, Agbu PA, Montgomery OL. Spectral differentiation of surface soils and soil properties: is it possible from space plataforms? Soil Sci 1993; 155: 283-93.

[10] Baret F, Jacquemound S, Hanocoq JF. The soil line concept in remote sensing. Remote Sens Environ 1993; 7: 1-18.

[11] Tanré D, Holben BN, Kaufman YJ. Atmospheric correction algorithm for NOAA-AVHRR products: theory and application. IEEE Trans Geosci Remote Sens 1992; 30: 231-48.

[12] Vermote E, Tanré D, Herman M, Morcrette JJ. Second Simulation of the Satellite Signal in the Solar Spectrum (6S). 6S User Guide Version 1, LOA-USTL. Villeneuve d'Ascq: France 1995.

[13] Nanni MR, Demattê JAM. Soil line behavior obtained by laboratorial spectroradiometry for different soil classes. R Bras Ci Solo 2006; 30: 1031-8.

[14] ENVI 3.0. The Environment for Visualizing Images: User's Guide. Better Solutions Consulting LLC: Lafayette, Colorado 1997.

[15] Empresa Brasileira de Pesquisa Agropecuária (EMBRAPA). Normas e Critérios para Levantamentos Pedológicos. Rio de Janeiro: EMBRAPA/SNLCS 1996; p. 94.

[16] Camargo AO, Moniz AC, Jorge JA, Valadares JM. Métodos de Análise Química, Mineralógica E Física de Solos do IAC. IAC: Campinas: Brasil 1986.

[17] Raij B, Quaggio JA, Cantarella H, Ferreira ME, Lopes AS, Bataglia CO. Análise Química do Solo Para Fins de Fertilidade. Fundação Cargill: Campinas 1987.

[18] Jackson ML. Soil chemical analysis: advanced course. Wisconsin University: Madison 1969.

[19] SAS INSTITUTE. SAS Software: User's Guide, Version 8.2. Cary 1999.

[20] White K, Walden J, Drake N, Eckardt F, Settle J. Mapping the iron oxide content of dune sands, Namib Sand Sea, Namíbia, using landsat thematic mapper data. Remote Sens Environ 1997; 62: 30-9.

[21] Madeira Netto JS. Spectral reflectance properties of soils. Photo Interpret 1996; 34: 59-70.

[22] Hunt GR, Salisbury JW, Lenhoff CJ. Visible and near-infrared spectra of minerals and rocks: III. Oxides and hydroxides. Mod Geol 1971; 2: 195-205.

[23] Demattê JAM, Garcia GJ. Alteration of soil properties through a weathering sequence as evaluated by spectral reflectance. Soil Sci Soc Am J 1999; 63: 327-42.

[24] Sherman LC, Waite TD. Electronic spectra of Fe3+ oxides and hydroxides in the near IR to near UV. Am Mineralogist 1985; 70: 1262-9.

[25] Demattê JAM, Focht D. Detecção de solos erodidos pela avaliação de dados espectrais. R Bras Ci Solo 1999; 23: 401-13.

[26] Kosmas CS, Curi N, Bryant RB, Franzmeier DP. Characterization of iron oxide minerals by second-derivative visible spectroscopy. Soil Sci Soc Am J 1984; 48: 401-5.

[27] Schwertmann U. Iron oxides in soil. Minerals in soils environments. Soil Sci Soc Am J 1989; 8: 379-465.

[28] Post DF, Horvath EH, Lucas WM, White SA, Ehasz MJ, Batchily AK. Relationship between soil color and Landsat reflectance on semiarid Rangelands. Soil Sci Soc Am J 1994; 58: 1809-16.

[29] Coleman TL, Agbu PA, Montgomery OL, Goot T, Prasad S. Spectral band selection for quantifying selected properties in highly weathering soils. Soil Sci 1991; 151: 355-61.

[30] Coleman TL, Tadesse W. Differentiating soil physical properties from multiple band DOQ data. Soil Sci 1995; 160: 81-91.

[31] Demattê JAM, Nanni MR. Weathering sequence of soils developed from basalt as evaluated by laboratory (IRIS), airborne (AVIRIS) and orbital (TM) sensors. Int J Remote Sens 2003; 24: 4715-38.

[32] Galvão LS, Vitorello I. Variability of laboratory measured soil lines of soils from southeastern Brazil. Remote Sens Environ 1998 ; 63 : 166-81.

[33] Melvin SB, Henly JP. Spectral characteristics of selected soils and vegetation in Northern Nevada and their discrimination using band ratio techniques. Remote Sens Environ 1987; 23: 155-75.

Received: January 29, 2009 Revised: February 5, 2009 Accepted: March 25, 2009